ISSN 2616-5791 Vol.4, Issue 5: 37-48, DOI: 10.25236/AJMHS.2023.040507

Theoretical Study on the Binding Properties of Inhibitors to Myeloid Cell Leukemia 1

Youxin Cui

School of Physics and Electronics, Shandong Normal University, Jinan, China

Abstract: *Myeloid leukemia 1 (Mcl-1) is a key anti-apoptotic member of the Bcl-2 protein family, and its overexpression or upregulation has been found in numerous cancer cells, which not only leads to tumorigenesis mediated by apoptotic escape modality, but also causes resistance to multiple subsequent anti-cancer therapies. The development of small molecule inhibitors that specifically target Mcl-1 and restore the blocked apoptotic pathway in cancer cells has emerged as a realistic solution for oncology drug design. Therefore, an in-depth study of the mechanism of action of inhibitors with Mcl-1 is important for the design of efficient drugs targeting Mcl-1. In this study, using molecular dynamics (MD) simulations, correlation analysis and principal component analysis, we revealed that the binding of inhibitors significantly altered the kinetic behavior of Mcl-1 and led to a conformational rearrangement of Mcl-1. Subsequently, the molecular mechanics-generalized Born surface area (MM-GBSA) method was used to further explore the binding ability of different inhibitors to Mcl-1, and the results showed that the calculated binding free energies agreed well with the experimental values, and van der Waals interactions and electrostatic interactions provided the main favorable contribution in the binding of inhibitors to Mcl-1. Furthermore, the interaction analysis showed a large number of hydrophobic interactions and hydrogen bonding between the inhibitor and Mcl-1. Finally, the residues F228, M231, M250, V253, T266, L267 and F270 and R263 were identified by residue-based free energy decomposition calculations to provide important energetic contributions to the binding of the inhibitor to Mcl-1 and could be key targets for the design of Mcl-1 inhibitors.*

Keywords: *Molecular dynamics simulation; Principal component analysis; Mcl-1; MM-GBSA; Cross correlation analysis*

1. Introduction

The process of normal development of the organism and removal of unwanted or damaged cells is known as apoptosis. Through cell proliferation and apoptosis, the cells of various tissues in the organism maintain their normal number and function.[1] It has been found that downregulation of apoptosis levels is closely related to tumor development and resistance to subsequent treatment.[2,3] As a major regulator of apoptosis, Bcl-2 family proteins play an important role in the apoptosis mechanism.[4-6] Generally, according to their structures and functions, Bcl-2 family proteins can be divided into two major groups: (1) anti-apoptotic protein members, such as Mcl1, Bcl-XL, Bcl-2 and Bcl-W; (2) pro-apoptotic protein members, which are further divided into multi-structural domain effector proteins containing multiple BH homologous structural domains, such as Bax, Bak, and Bcl-xs, and BH3-only proteins with only one BH3 homologous structural domain, such as Bim, Bid, and Bad.[7,8] The common structural feature of Bcl-2 protein family members is the conserved BH3 structural domain, and they interact through this common BH3 structural domain to control the permeability of the outer mitochondrial membrane, regulate the release of apoptotic factors, and thus regulate apoptosis.[9-16]

Mcl-1 is a key anti-apoptotic protein in the Bcl-2 family whose role in tumorigenesis and maintenance has been demonstrated in various genetic mouse models and has been found to be overexpressed in a variety of human cancers, including breast, lung, prostate, pancreatic, cervical, and leukemia.[17-27] Although it does not directly promote tumor cell proliferation, high expression of Mcl-1 promotes tumorigenesis and progression in another form-anti-apoptosis. Mcl1 overexpression also leads to resistance to oncology drug therapy with Bcl-2 selective inhibitors and other small molecule drugs.[28-32] Therefore, down-regulation of Mcl1 expression not only inhibits tumor development but is also essential to overcome drug resistance in tumor therapy.

As the mechanisms by which the Bcl-2 protein family regulates apoptosis have been explored, it has been revealed that apoptosis is mediated by the permeabilization of the outer mitochondrial membrane

ISSN 2616-5791 Vol.4, Issue 5: 37-48, DOI: 10.25236/AJMHS.2023.040507

which induced by the activation of Bax and Bak to form homo- or heterodimers.[16,33,34] Mcl-1 protein prevents the initiation of the apoptotic program and maintains cell survival by binding to and preventing the dimerization of the pro-apoptotic effector proteins Bax and Bak, or by isolating the "activator" BH3-only protein, which leaves the effector proteins Bax and Bak in an inactive state.[35,36] By using small molecule inhibitors that compete with pro-apoptotic proteins for binding in the hydrophobic BH3 binding pocket of Mcl-1 protein, Mcl-1 can be effectively prevented from binding to BAX or BAK or cleave their dimerization complexes, thereby relieving the apoptosis-inhibiting function of Mcl-1, restoring the blocked apoptotic pathway in cancer cells, and inducing apoptosis to remove cancerous cells. Therefore, it is essential to develop efficient inhibitors that can specifically target Mcl-1 and down-regulate its activity.

In this work, molecular dynamics simulations were used to investigate the interaction mechanism of Mcl-1 with existing binding partners at the atomic level, to explore the protein conformational changes and to identify the key inhibitor binding sites. We selected five inhibitors 19H, 4M6, 6AK, CN7 and ECM, and the structures of Mcl-1 protein and five small molecule inhibitors are shown in Figure 1A-F, respectively. The five inhibitors 19H, 4M6, 6AK, CN7 and ECM showed different levels of binding ability to Mcl-1, and the elucidation of the molecular mechanisms underlying the differences in the binding ability of the different inhibitors is essential for the development of efficient inhibitors of Mcl-1. In this study, we used MD simulations,[37,38] molecular mechanics generalized Born surface area (MM-GBSA) method,[39,40] principal component analysis (PCA)[41,42] and dynamic correlation maps (DCCMs)[43,44] to analyze the details of the conformational changes of Mcl-1 and the binding mechanism of inhibitors to Mcl-1. We also hope that this study provides theoretical guidance for the design of more efficient and specific Mcl-1 inhibitors.

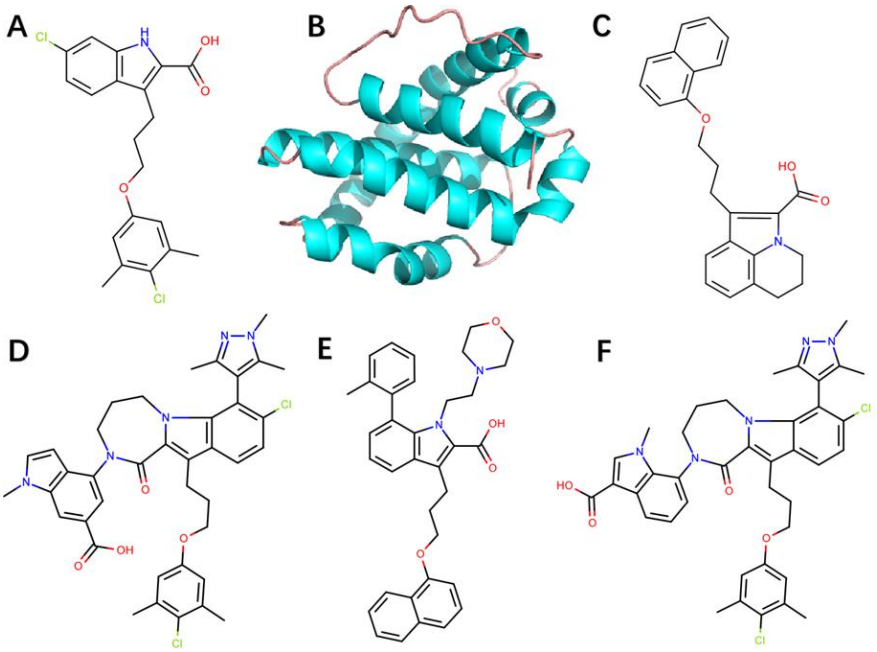

Figure 1: Molecular structures of Mcl-1 protein and five inhibitors: (A) 19H, (B) Mcl-1, (C) 4M6, (D) 6AK, (E) CN7, (F) ECM. Mcl-1 and inhibitors are shown in cartoon and line modes, respectively.

2. Materials and methods

2.1. Construction of initial systems

The initial coordinates of Mcl-1 complexes with the five inhibitors 19H, 4M6, 6AK, CN7 and ECM were obtained from the Protein Data Bank (PDB ID: 4HW2, 4ZBI, 5IF4, 6B4U and 6BW8). All crystalline water molecules identified in the crystal structure of the inhibitor-Mcl-1 complex were retained in the initial model. The structures of 19H, 4M6, 6AK, CN7, and ECM were optimized at the semi-empirical AM1 level and subsequently assigned BCC charges to each atom of the inhibitor by the Antechamber module in Amber.[45,46] The six simulated systems were parameterized using the Leap module in Amber 18 to (1) construct the missing chemical bonds between the hydrogen and heavy atoms in the crystal structure, (2) derive the force field parameters for the protein and inhibitor using ff14SB

ISSN 2616-5791 Vol.4, Issue 5: 37-48, DOI: 10.25236/AJMHS.2023.040507

and the generalized Amber force field (GAFF),[47-49] respectively, and (3) use the TIP3P model for water molecule were assigned and then six systems were dissolved in the octahedral water tank of the TIP3P model and the system was placed in a cubic periodic box extending 12 Å outward from each dimension of the solute surface, (4) appropriate amounts of counter ions (Na+ and Cl-) were added to neutralize each system to obtain the neutral system.

2.2. Molecular Dynamics Simulations

The initialization of the simulated system forms bad inter-atoms contacts that can lead to MD simulation instability. To eliminate these adverse effects, a two-stage energy minimization was performed to optimize these six systems, namely a steepest descent minimization in 2500 steps and a conjugate gradient minimization in 2500 steps. Subsequently, the temperature of these six systems was gradually heated from 0 K to 300 K, and the system temperature was maintained at a constant temperature of 300 K. Kinetic equilibrium simulations were performed for 2 ns. Finally, the optimized structure was used as the starting structure for MD simulations, and 300 ns unconstrained MD simulations were run for these six systems at a constant temperature of 300 K and at a constant pressure of 1 atm. Meanwhile, the atomic coordinates of the systems were recorded every 2 ps for subsequent processing analysis. During the simulations, the temperature was kept at 300 K using a Langevin thermostat, the SHAKE algorithm (with a time step of 2 fs) was used to constrain all chemical bonds involving hydrogen atoms,[50,51] and the particle grid Ewald (PME) method was used to calculate long-range electrostatic interactions. To calculate the near-range electrostatic interactions and van der Waals interactions, the cutoff distance was set to 10 Å.[52,53] The MD simulations for all six systems were run using the pmemd.cuda module of Amber18.[54-56]

2.3. Calculations of binding free energies

The binding free energy is an important indicator of the binding strength of inhibitors to proteins, which is important for the rational design of efficient inhibitors targeting proteins.[57-61] Molecular mechanics-generalized Born surface area (MM-GBSA) is a fast and reliable method to measure the binding ability of inhibitors to proteins. In the calculation, all water molecules and ions were removed. The binding free energy (ΔG) can be described as:

$$\Delta G = G_{complex} - (G_{protein} + G_{inhibitor}) \quad (1)$$

where $G_{complex}, G_{protein}$ and $G_{inhibitor}$ represent the free energy of the complex, the free energy of the receptor protein and the free energy of the small molecule inhibitor, respectively. And the binding free energy ΔG can be calculated from the sum of the gas-phase binding energy of the molecular mechanism (ΔE_{MM}), the solventization free energy (ΔG_{solv}) and the change in entropy ($-T\Delta S$) as follows:

$$\Delta G = \Delta E_{MM} + \Delta G_{solv} - T\Delta S \quad (2)$$

where ΔE_{MM} consists of electrostatic interaction energy (ΔE_{ele}) and van der Waals interaction energy (ΔE_{vdw}). The solvation free energy (ΔG_{solv}) consists of polar solvation free energy (ΔG_{pol}) and non-solvation free energy (ΔG_{nonpol}). Thus, the binding free energy ΔG can be further expressed as the following equation:

$$\Delta G = \Delta E_{ele} + \Delta E_{vdw} + \Delta G_{pol} + \Delta G_{nonpol} - T\Delta S \quad (3)$$

Usually, the first two terms ΔE_{ele} and ΔE_{vdw} can be calculated by molecular mechanics, and the polar solvation free energy ΔG_{pol} term can be solved by the generalized Bonn model. The nonpolar solvation free energy ΔG_{nonpol}, on the other hand, can be calculated using the following equation:

$$\Delta G_{nonpol} = \gamma \times \Delta SASA + \beta \quad (4)$$

where γ is the surface tension and its value is set to 0.0072 kcal/mol·Å-2 and the value of β is 0.00 kcal/mol . $\Delta SASA$ denotes the surface area accessible to the solvent,[62] the atomic radius is set with reference to the radius in the prmtop file, and the default dielectric constants are 1.0 and 80.0 for the internal solute and the external solvent, respectively. The last term ($-T\Delta S$) denotes the contribution of the entropic change to the binding free energy, and this component is calculated using classical statistical thermodynamics and Normal Mode analysis.[63]

ISSN 2616-5791 Vol.4, Issue 5: 37-48, DOI: 10.25236/AJMHS.2023.040507

3. Results and discussion

3.1. Internal dynamics of Mcl-1 induced by inhibitor binding

To investigate the internal kinetic changes induced by inhibitor binding, 300 ns molecular dynamics simulations were performed for the free state Mcl-1 system and the 19H, 4M6, 6AK, CK7 and ECM complexes with protein binding. Subsequently, the root-mean-square deviation (RMSD) of the backbone atoms relative to the crystal structure in these six systems was calculated over time to assess the stability of the simulated systems (Figure 2). After 150 ns of MD simulations, the six systems basically reached equilibrium. According to Figure 2, the mean RMSD values of Mcl-1, 19H/Mcl-1, 4M6/Mcl-1, 6AK/Mcl-1, CN7/Mcl-1, and ECM/Mcl-1 in the free state were 1.80, 1.08, 1.01, 0.91, 0.93, and 1.14 Å, respectively. Meanwhile, the RMSD fluctuations of all systems after equilibrium were in the range of less than 1 Å. This result indicates that the RMSD fluctuations of all systems after equilibrium were less than 1 Å. This result indicates that the equilibrium and stability of the MD simulations are reliable, and thus can be used for subsequent processing analysis.

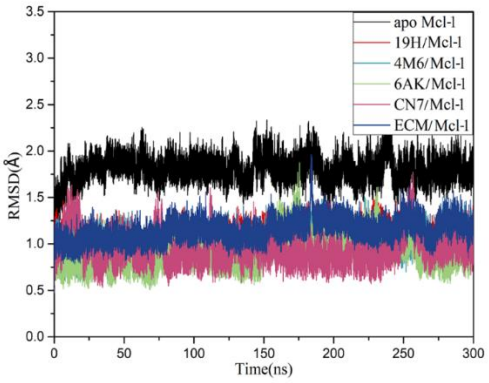

Figure 2: Evolution of root mean square deviations (RMSD) of Mcl-1backbone atoms as the simulation time.

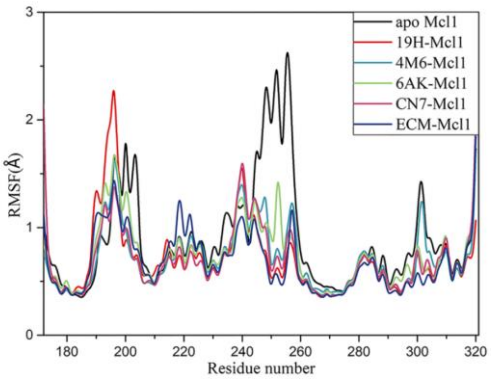

Figure 3: Root-mean-square fluctuations (RMSF) of Cα atoms, used to evaluate the structural flexibility of Mcl-1.

The root mean square fluctuation (RMSF) is a reasonable indicator of the structural flexibility of the protein. Therefore, the RMSF of the Cα atom in Mcl-1 was calculated to understand the effect of inhibitor binding on the structural flexibility of Mcl-1 (Figure 3). The results showed that the RMSF values near residues 200, 231, 250, 254, 258 and 263 were largely reduced, indicating that the flexibility of Mcl-1 in these regions was restricted upon inhibitor binding. Differently, 19H binding significantly enhanced the flexibility in the regions near residues 190, 195, and 240, and ECM binding also increased the RMSF values in the regions near residues 190, 195, 218, and 223. In contrast, binding of 4M6, 6AK and CN7 to Mcl-1 completely inhibited the flexibility of these regions. The binding of the five inhibitors resulted

ISSN 2616-5791 Vol.4, Issue 5: 37-48, DOI: 10.25236/AJMHS.2023.040507

in high and low fluctuations of Mcl-1, and the ranking from high to low was consistent with the subsequent ranking of the binding energy values. This clearly explains that inhibitors with lower binding affinity interact moderately or weakly with binding site residues and thus cause more fluctuations. In contrast, inhibitors with higher binding affinity have tight and stable interactions with binding site residues, resulting in less fluctuations of Mcl-1. Taken together, it is shown that the binding of inhibitors generally inhibits the movement of Mcl-1, which favors the stability of the complex structure, and that the presence of 19H, 4M6, 6AK, CN7 and ECM has different effects on the structural structure flexibility of Mcl-1.

3.2. Conformational changes of Mcl-1 induced by inhibitor binding

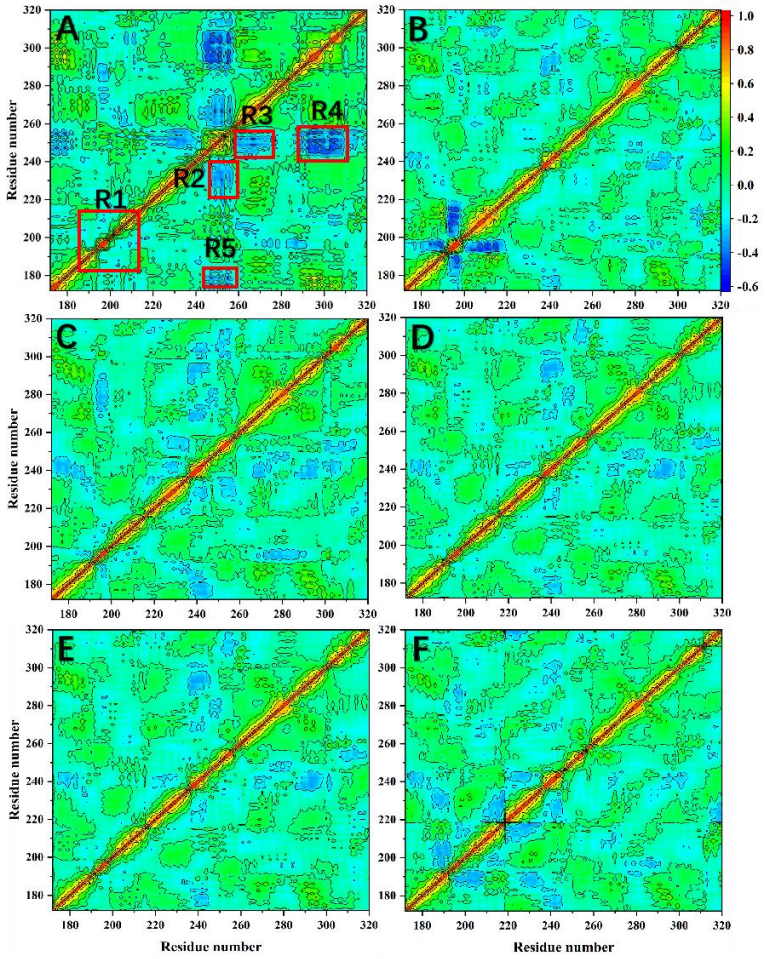

Figure 4: Cross-correlation maps reflecting relative motions between residues of MCL-1: (A) the apo Mcl-1, (B) the 19H/Mcl-1, (C) the 4m6/Mcl-1, (D) the 6AK/Mcl-1, (E) the CN7/Mcl-1, (F) the ECM/Mcl-1.

To further understand the changes in internal dynamics caused by inhibitor binding to Mcl-1, inter-correlation diagrams depicting atomic fluctuations were calculated using the CPPTRAJ program in Amber (Figure 4). The regions marked in red and yellow indicate strong positive correlation motions between residues, while the regions highlighted in blue and black indicate strong anti-correlation motions between residues. The diagonal regions reflect the motion of residues relative to themselves, while the non-diagonal regions reflect the mutual motion of different residues. Overall, the presence of inhibitors has different effects on the movement pattern of Mcl-1.

For the correlation matrix of free state Mcl-1, the R1 region depicts a positive correlation motion between residues 180-210, while the R2, R3, R4 and R5 regions present an anti-correlation motion between residues. The binding of the inhibitor has a significant effect on the correlated motion of Mcl-1 compared to the free state Mcl-1 (Figure 4B-F). As can be seen from Figure 4, the binding of inhibitors results in an overall weakening of the correlated motion between residues, which means that the structure of the system with inhibitor binding is more stable. However, the binding of different inhibitors also

ISSN 2616-5791 Vol.4, Issue 5: 37-48, DOI: 10.25236/AJMHS.2023.040507

brings different patterns of motion to the Mcl-1 protein. For the 19H/Mcl-1 complex, inhibitor binding enhanced the anti-associative motion of the R1 region while inhibiting the anti-associative motion of the R2, R3, R4 and R5 regions (Figure 4B). For the 4M6/Mcl-1 complex, the binding of 4M6 to Mcl-1 barely changed the kinetic behavior of the R1 region in Mcl-1, but significantly inhibited the anticorrelated motions of the R2, R3, R4 and R5 regions in Mcl-1 (Figure 4C). Similar to the 4M6/Mcl-1 complex, the presence of 6AK and CN7 in the 6AK/Mcl-1 and CN7/Mcl-1 complexes inhibited the anti-correlated motions of the R2, R3, R4 and R5 regions in Mcl-1, but did not significantly alter the kinetic behavior of the R1 region (Figure 4D and E). For the ECM/Mcl-1 complex, the binding of ECM slightly enhanced the anti-correlation motion of the R1 region while inhibiting the anti-correlation motion of the R2-R5 region (Figure 4F). The above analysis suggests that inhibitor binding has a significant effect on the mode of movement of Mcl-1 and that the difference in internal kinetics reflects the change in the relative position of key residues induced by inhibitor binding.

3.3. Evaluation of the binding ability of inhibitors to Mcl-1

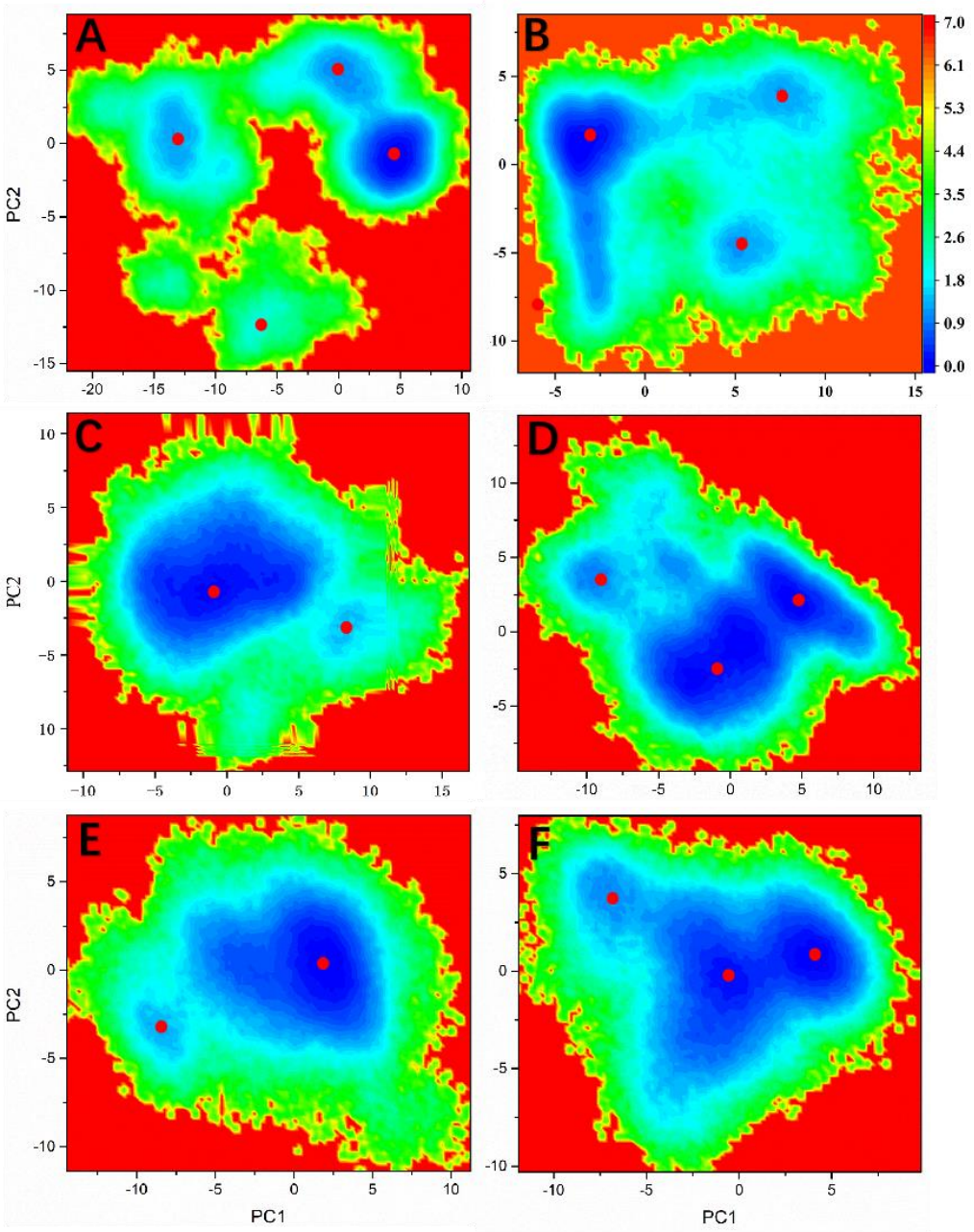

Figure 5: Free energy landscapes of Mcl-1 projected on the first two eigenvectors: (A) the apo Mcl-1, (B) the 19H/Mcl-1, (C) the 4m6/Mcl-1, (D) 6AK/Mcl-1, (E) CN7/Mcl-1, (F) ECM/Mcl-1.

ISSN 2616-5791 Vol.4, Issue 5: 37-48, DOI: 10.25236/AJMHS.2023.040507

We also explored the conformational changes of Mcl-1 using the free energy landscape, which plays an important role in understanding the energetic basis of the conformational space changes of Mcl-1. To achieve this goal, the free energy landscape was constructed using the projections of the first two eigenvectors PC1 and PC2 on the MD trajectory (Figure 5). As shown in Figure 5A, for the free state Mcl-1 system, four energy basins were detected by MD simulations, indicating that the conformational distribution of Mcl-1 is mainly in these four subspaces (Figure 5A). The binding of inhibitors 19H, 4M6, 6AK, CN7 and ECM to Mcl-1 resulted in the conformational redistribution of Mcl-1 in three, two, three, two and three energy basins, indicating that the Mcl-1 conformation was concentrated in three, two, three, two and three subspaces bound by 19H, 4M6, 6AK, CN7 and ECM, respectively (Figure 5(B-E)). The above analysis showed that the binding to different structural inhibitors significantly affected the conformation of Mcl-1 and that the binding of inhibitors made the conformation of Mcl-1 more stable.

To evaluate the difference in the binding ability of 19H, 4M6, 6AK, CN7 and ECM to Mcl-1, we calculated the free energy of binding of five inhibitors to Mcl-1 using the MM-GBSA method. Due to the long time to calculate the entropy change, we extracted 50 conformations from 200 conformations to calculate the role of entropy in inhibitor binding. The results of MM-GBSA calculation are shown in Table 1.

According to Table 1, it can be seen that our calculated binding free energies are in good agreement with the experimental values and are in agreement with the experimental value ordering, indicating that our present analysis of the free energies is reliable and reasonable. The binding free energies of 19H, 4M6, 6AK, CN7 and ECM with Mcl-1 were -17.29, -11.76, -20.38, -18.78 and -19.00 kcal/mol, with 6AK binding to Mcl-1 being the strongest. As shown in Table 1, the binding free energy consisted of electrostatic interaction (ΔE_{ele}), van der Waals interaction (ΔE_{vdW}), polar solvation free energy (ΔG_{gb}), nonpolar solvation free energy (ΔG_{nonpol}) and entropy change ($-T\Delta S$). Among the five systems, van der Waals interactions and electrostatic interactions contribute high favorable energies for complex formation, in addition, the nonpolar solvation free energy also contributes favorable energies for inhibitor binding, but to a lesser extent. In contrast, the polar solvation free energy and entropy changes provide unfavorable effects on the binding of inhibitors. The above analysis suggests that van der Waals interactions and electrostatic interactions provide the main favorable contributions in the binding of inhibitors to Mcl-1 and are key factors in the development of efficient inhibitors designed for Mcl-1.

Table 1: Binding free energies of inhibitors to Mcl-1calculated by MM-GBSA method.

Components	**19H/Mcl-1**		**4M6/Mcl-1**		**6AK/Mcl-1**		**CN7/Mcl-1**		**ECM/Mcl-1**	
	Mean	σ[b]	Mean	σ[b]	Mean	σ[b]	Mean	σ[b]	Mean	σ[b]
ΔE_{ele}	-29.54	10.62	-19.74	7.96	-40.90	4.81	-40.92	6.51	-11.05	7.77
ΔE_{vdw}	-48.20	4.06	-41.38	3.44	-49.88	3.12	-44.52	3.03	-43.58	3.37
ΔG_{pol}	47.64	9.25	38.32	7.85	55.27	4.43	54.40	5.49	22.79	6.99
ΔG_{nonpol}	-5.91	0.24	-5.49	0.27	-5.98	0.14	-5.81	0.16	-5.44	8.18
$\Delta G_{ele+pol}$[c]	18.10	3.43	18.58	3.41	14.37	3.02	13.48	3.36	11.74	3.14
$-T\Delta S$	18.72	6.21	16.54	3.64	21.11	5.58	18.07	6.43	18.28	5.08
ΔG_{bind}[d]	-17.29		-11.76		-20.38		-18.78		-19.00	
ΔG_{exp}[e]	-9.96		-8.932		-12.76		-11.04		-12.6078	

[a] *All components of free energies are in kcal/mol.*
[b] *Standard errors of means.*
[c] $\Delta G_{ele+pol} = \Delta E_{ele} + \Delta G_{pol}$
[d] $\Delta G_{bind} = \Delta E_{ele} + \Delta E_{vdw} + \Delta G_{pol} + \Delta G_{nonpol} - T\Delta S$
[e] *The experimental values were derived from the experimental IC50 values using the equation:* $\Delta G_{exp} = -RTlnIC_{50}$

3.4. Hot spot residues of inhibitor-Mcl-1 binding

To gain more insight into the molecular mechanism of binding of 19H, 4M6, 6AK, CN7 and ECM to Mcl-1, the energy contribution of individual residues at the binding interface of the inhibitor to Mcl-1 was investigated using a residue-based free energy decomposition approach. Figure 6 show the key residues bound to the inhibitor, which provide the major energy contributions to the binding of 19H, 4M6, 6AK, CN7, and ECM to Mcl-1. The lowest energy structure generated by the MD trajectory was used to depict the geometric information of inhibitor-residue interactions (Figure 7). Also, the corresponding information on the hydrogen bonding interaction of the inhibitor with Mcl-1 was displayed in Table 2

ISSN 2616-5791 Vol.4, Issue 5: 37-48, DOI: 10.25236/AJMHS.2023.040507

using the CPPTRAJ module in Amber18. The decomposition analysis provided strong information for the discovery of the major energy contributing residues. A closer study at the Mcl-1 binding site showed that the collection of hydrophobic and polar residues exhibited significant variations in energy distribution (Figure 7).

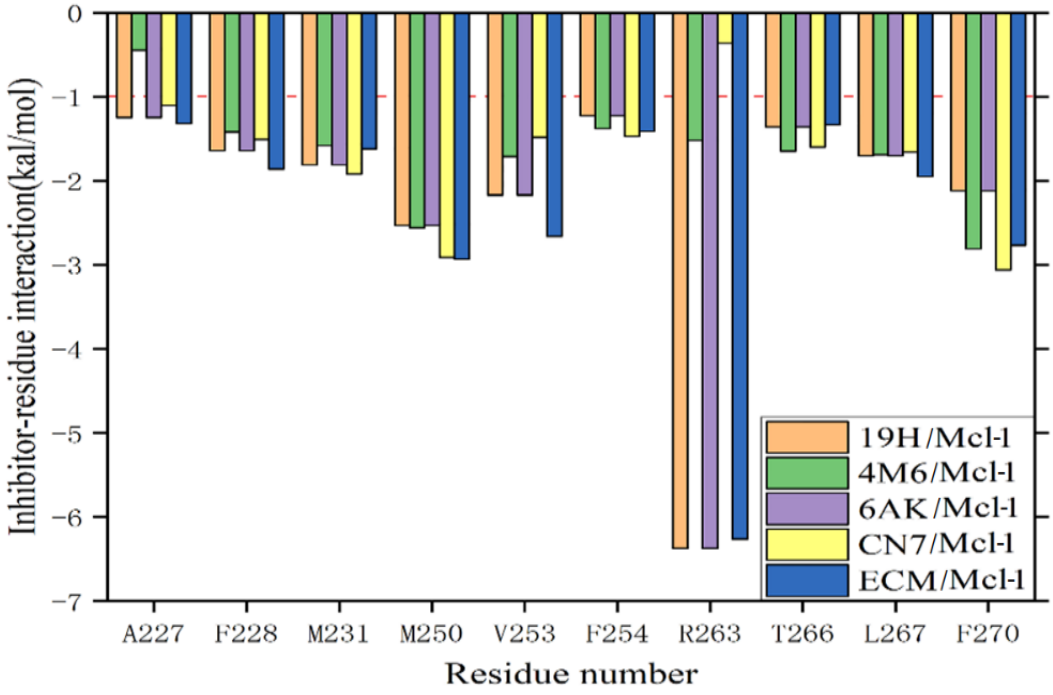

Figure 6: Interaction energies of three inhibitors 19H, 4M6, 6AK, CN7 and ECM with key residues in Mcl-1.

Table 2: Main hydrogen bonding interactions of three inhibitors with MCL-1.

Components	Hydrogen bonds[a]	Distance(Å)	Angle (deg)	Occupancy (%)[b]
19H/Mcl-1	[c]R263-NH2-HH21···19H-OAD	2.94	145.4	17.95
	R263-NE-HE···19H-OAD	3.21	145.4	8.73
4M6/Mcl-1	R263-NE-HE···4M6-OAB	3.07	150.0	9.38
	R263-NE-HE···4M6-OAA	3.08	143.8	8.15
6AK/Mcl-1	R263-NE-HE···6AK-O02	2.90	158.9	96.91
	R263-NH2-HH21···6AK-O02	3.20	135.0	18.65
	V258-N-H···6AK-O03	3.13	145.2	12.59
	V258-N-H···6AK-O04	3.20	146.4	8.42
CN7/Mcl-1	R263-NH1-HH11···CN7-O38	3.03	139.7	14.93
	R263-NE-HE···CN7-O38	3.22	142.1	8.45
ECM/Mcl-1	R263-NE-HE···ECM-O33	2.93	155.6	94.76
	N260-ND2-HD21···ECM-O29	2.98	147.2	55.63
	R263-NH2-HH21···ECM-O33	3.33	129.5	9.57

[a] *Hydrogen bonds are determined by the acceptor . . . donor distance of <3.5 Å and acceptor. H-donor angle of >120°.*
[b] *Occupancy (%) is defined as the percentage of simulation time that a specific hydrogen bond exists.*
[c]*The full line indicates an atom belonging to a certain residue or linking to the other atoms, and the dotted line represents the formation of a hydrogen bonding interaction.*

ISSN 2616-5791 Vol.4, Issue 5: 37-48, DOI: 10.25236/AJMHS.2023.040507

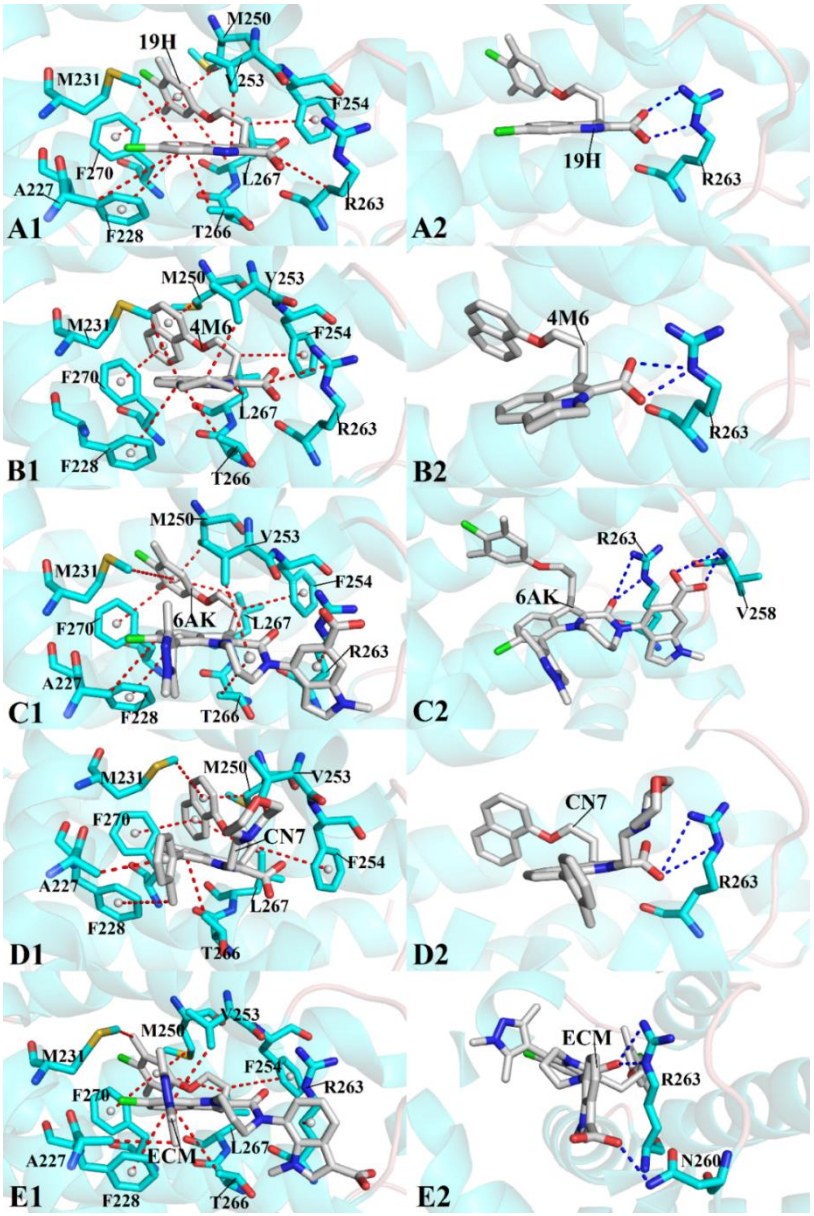

Figure 7: Geometric information of inhibitors relative to key residues in the Mcl-1

As shown in Figure 6, ten key residues, A227, F228, M231, M250, V253, F254, R263, T266, L267, and F270, contribute >1 kcal/mol of free energy to the binding of the inhibitor to Mcl-1. To further understand the relative energy contribution between the contacting residues, the binding free energies obtained for the five inhibitor complexes were compared (Figure 6). For 19H/Mcl-1, residues A227, M231, M250, V253, F254, T266 and L267 formed CH-π interactions, residues F228 and F270 formed π-π interactions and residue R263 formed CH-CH interactions. Two hydrogen bonds with 17.95% and 8.73% occupancy were formed between residue R263 and the inhibitor (Figure 7A and Table 2). For 4M6/Mcl-1, residues M231, M250, V253, F254, T266 and L267 formed CH-π interactions, residues F228 and F270 formed π-π interactions, and residue R263 formed CH-CH interactions. Two hydrogen bonds with occupancies of 9.38% and 8.15%, respectively, were formed between residues R263 and the inhibitor (Figure 7B and Table 2). For 6AK/Mcl-1, residues A277, M231, M250, V253, F254, R263, T266, and L267 formed CH-π interactions, and residues F228 and F270 formed π-π interactions. Two hydrogen bonds with occupancies of 96.91% and 18.65%, respectively, were formed between residues R263 and the inhibitor, and two hydrogen bonds with occupancies of 12.59% and 8.42%, respectively, were formed by residue V258 (Figure 7C and Table 2). For CN7/Mcl-1, residues A277, M231, M250, V253, F254, T266 and L267 formed CH-π interactions, and residues F228 and F270 formed π-π interactions. Two hydrogen bonds with 14.93% and 8.45% occupancy, respectively, were formed between residues R263 and the inhibitor (Figure 7D and Table 2). For ECM/Mcl-1, residues A277, M231, M250, V253, F254, R263, T266 and L267 formed CH-π interactions, and residues F228 and F270 formed

ISSN 2616-5791 Vol.4, Issue 5: 37-48, DOI: 10.25236/AJMHS.2023.040507

π-π interactions. Two hydrogen bonds with 94.76% and 9.57% occupancy, respectively, were formed between residues R263 and the inhibitor, and one hydrogen bond with 55.63% occupancy, respectively, was formed by residue N260 (Figure 7E and Table 2).

4. Conclusions

In this work, the conformational changes and binding modes induced by the binding of Mcl-1 to five inhibitors, 19H, 4M6, 6AK, CN7 and ECM, were investigated in depth. In particular, we performed 300 ns MD simulations of the complexes of Mcl-1 and five inhibitors (19H, 4M6, 6AK, CN7 and ECM) and explored the effect of inhibitor binding on the conformational changes of Mcl-1. Correlation matrices describing atomic fluctuations and PC analysis were calculated to explore the internal dynamics of Mcl-1 due to inhibitor binding. The results showed that the binding of Mcl-1 protein to inhibitors significantly changed the motion direction and intensity of certain residues. Further binding free energies calculated using the MM-GBSA method suggest that van der Waals interactions and electrostatic interactions play an important role in inhibitor binding. The residue-based free energy decomposition method elucidated the contribution of individual residues in the inhibitor binding process. The hydrophobic rings of the five inhibitors formed strong CH-π interactions and π-π interactions with residues F228, M231, M250, V253, T266, L267 and F270. The findings of this study can provide valuable guidance for the design of novel Mcl-1 inhibitors and provide a strong reference for iMcl-1ving the specificity and efficacy of new generation chemotherapeutic drugs, as well as providing new ideas for addressing future tumor therapy resistance and finding new therapeutic targets.

Acknowledgements

The authors declare no competing financial interest.

References

[1] Michael D. Jacobson, Miguel Weil, Martin C. Raff. Programmed Cell Death in Animal Development. Cell, 1997, 88(3): 347-354.
[2] Douglas Hanahan, Robert A. Weinberg. Hallmarks of Cancer: The Next Generation. Cell, 2011, 144(5): 646-674.
[3] Michael F., Tolkovsky A. M., Vilmante B., et al. Neuronal Cell Death. Physiological Reviews, 2018, 98(2): 813-880.
[4] V. V. Senichkin, A. Y. Streletskaia, B. Zhivotovsky and G. S. Kopeina, Molecular comprehension of Mcl-1: from gene structure to cancer therapy, Trends Cell Biol., 2019, 29, 549–562.
[5] P. E. Czabotar, G. Lessene, A. Strasser and J. M. Adams, Control of apoptosis by the BCL-2 protein family: implica-tions for physiology and therapy, Nat. Rev. Mol. Cell Biol., 2014, 15, 49–63.
[6] S. Shaw, Z. Bian, B. Zhao, J. C. Tarr, N. Veerasamy, K. O. Jeon, J. Belmar, A. L. Arnold, S. A. Fogarty, E. Perry and J. L. Sensintaffar, Optimization of potent and selective tricyclic indolediazepinone myeloid cell leukemia-1 inhibi-tors using structure-based design, J. Med. Chem., 2018, 61, 2410–2421.
[7] Youle R. J., Strasser A. The BCL-2 protein family: opposing activities that mediate cell death. Nature Reviews Molecular Cell Biology, 2008, 9(1): 47-59.
[8] Elkholi R., Floros K. V., Chipuk J. E. The Role of BH3-Only Proteins in Tumor Cell Development, Signaling, and Treatment. Genes & Cancer, 2011, 2(5):523-537.
[9] Maji S, Panda S, Samal SK, et al. Bcl-2 antiapoptotic family proteins and chemoresistance in cancer. Adv Cancer Res, 2018, 137: 37-75
[10] Westphal D., Dewson G., Czabotar P. E., et al. Molecular biology of Bax and Bak activation and action. Biochimica et biophysica acta, 2011, 1813(4): 521-31.
[11] Llambi F., Wang Y. M., Victor B., et al. BOK Is a Non-canonical BCL-2 Family Effector of Apoptosis Regulated by ER-Associated Degradation. Cell, 2016:421-433.
[12] N. N. Danial and S. J. Korsmeyer, Cell death: critical control point, Cell, 2004, 116, 205–219.
[13] J. C. Reed, Bcl-2 and the regulation of programmed cell death, J. Cell Biol., 1994, 124, 1–6.
[14] N. F. Pelz, Z. Bian, B. Zhao, S. Shaw, J. C. Tarr, J. Belmar, C. Gregg, D. V. Camper, C. M. Goodwin, A. L. Arnold and J. L. Sensintaffar, Discovery of 2-indole-acylsulfonamide myeloid cell leukemia 1 (Mcl-1) inhibitors using fragment-based methods, J. Med. Chem., 2016, 59, 2054–2066.
[15] S. Cory and J. M. Adams, The Bcl-2 family: regulators of the cellular life-or-death switch, Nat. Rev. Cancer, 2002, 2, 647–656.

ISSN 2616-5791 Vol.4, Issue 5: 37-48, DOI: 10.25236/AJMHS.2023.040507

[16] M. Bruncko, L. Wang, G. S. Sheppard, D. C. Phillips, S. K. Tahir, J. Xue, S. Erickson, S. Fidanze, E. Fry, L. Hasvold and G. J. Jenkins, Structure-guided design of a series of Mcl-1 inhibitors with high affinity and selectivity, J. Med. Chem., 2015, 58, 2180–2194.
[17] J. P. Burke, Z. Bian, S. Shaw, B. Zhao, C. M. Goodwin, J. Belmar, C. F. Browning, D. Vigil, A. Friberg, D. V. Camper and O. W. Rossanese, Discovery of tricyclic indoles that potently inhibit Mcl-1 using fragment-based methods and structure-based design, J. Med. Chem., 2015, 58, 3794–3805.
[18] Q. Ding, X. He, W. Xia, J. M. Hsu, C. T. Chen, L. Y. Li, D. F. Lee, J. Y. Yang, X. Xie, J. C. Liu and M. C. Hung, Myeloid cell leukemia-1 inversely correlates with glycogen synthase kinase-3b activity and associates with poor prognosis in human breast cancer, Cancer Res., 2007, 67, 4564–4571.
[19] T. Zhang, C. Zhao, L. Luo, H. Zhao, J. Cheng and F. Xu, The expression of Mcl-1 in human cervical cancer and its clinical significance, Med. Oncol., 2012, 29, 1985–1991.
[20] Beroukhim R, Mermel CH, Porter D, et al. The landscape of somatic copy-number alteration across human cancers. Nature. 2010; 463(7283): 899–905.
[21] Wei G, Margolin AA, Haery L, et al. Chemical genomics identifies small-molecule MCL-1 repressors and BCL-xL as a predictor of MCL-1 dependency. Cancer Cell. 2012; 21(4):547–562.
[22] Ding Q, He X, Xia W, et al. Myeloid cell leukemia-1 inversely cor-relates with glycogen synthase kinase-3beta activity and associates with poor prognosis in human breast cancer. Cancer Res. 2007; 67(10): 4564–4571.
[23] Song L, Coppola D, Livingston S, Cress D, Haura EB. Mcl-1 regulates survival and sensitivity to diverse apoptotic stimuli in human non-small cell lung cancer cells. Cancer Biol Ther. 2005; 4(3):267–276.
[24] Krajewska M, Krajewski S, Epstein JI, et al. Immunohistochemical analysis of bcl-2, bax, bcl-X, and Mcl-1 expression in prostate cancers. Am J Pathol. 1996; 148(5):1567–1576.
[25] Miyamoto Y, Hosotani R, Wada M, et al. Immunohistochemical analy-sis of Bcl-2, Bax, Bcl-X, and Mcl-1 expression in pancreatic cancers. Oncology. 1999;56(1):73–82.
[26] Brotin E, Meryet-Figuiere M, Simonin K, et al. Bcl-XL and MCL-1 constitute pertinent targets in ovarian carcinoma and their concomi-tant inhibition is sufficient to induce apoptosis. Int J Cancer. 2010; 126(4):885–895.
[27] Derenne S, Monia B, Dean NM, et al. Antisense strategy shows that Mcl-1 rather than Bcl-2 or Bcl-x(L) is an essential survival protein of human myeloma cells. Blood. 2002; 100(1):194–199.
[28] I. E. Wertz, et al., Sensitivity to antitubulin chemotherapeu-tics is regulated by MCL-1 and FBW7, Nature, 2011, 471, 110–114.
[29] S. H. Wei, K. Dong, F. Lin, X. Wang, B. Li, J. J. Shen, Q. Zhang, R. Wang and H. Z. Zhang, Inducing apoptosis and enhancing chemosensitivity to gemcitabine via RNA interference targeting MCL-1 gene in pancreatic carcinoma cell, Cancer Chemother. Pharmacol, 2008, 62, 1055–1064.
[30] S. H. Kim, M. S. Ricci and W. S. El-Deiry, MCL-1: a gateway to TRAIL sensitization, Cancer Res., 2008, 68, 2062–2064.
[31] S. K. Tahir, X. Yang, M. G. Anderson, S. E. Morgan-Lappe, A. V. Sarthy, J. Chen, R. B. Warner, S. C. Ng, S. W. Fesik, S. W. Elmore, S. H. Rosenberg and C. Tse, Influence of BCL-2 family members on the cellular response of small-cell lung cancer cell lines to ABT-737, Cancer Res., 2007, 67, 1176–1183.
[32] Wei SH, Dong K, Lin F, et al. Inducing apoptosis and enhancing chemosensitivity to gemcitabine via RNA interference targeting Mcl-1 gene in pancreatic carcinoma cell. Cancer Chemother Pharmacol. 2008;62(6):1055–1064.
[33] Pawlowski J., Kraft A. S. Bax-induced apoptotic cell death. Proceedings of the National Academy of Sciences of the United States of America, 2000, 97(2):529-529.
[34] Westphal D., Dewson G., Czabotar P. E., et al. Molecular biology of Bax and Bak activation and action. Biochimica et biophysica acta, 2011, 1813(4): 521-31.
[35] M. R. Arkin and J. A. Wells, Small-molecule inhibitors of protein-protein interactions: progressing towards the dream, Nat. Rev. Drug Discovery, 2004, 3, 301–317.
[36] Vogler M. BCL2 A1: The underdog in the BCL2 family. Cell Death Differ, 2012, 19(1): 67-74.
[37] Dror R. O., Dirks R. M., Grossman J. P., et al. Biomolecular Simulation: A Computational Microscope for Molecular Biology. Annual Review of Biophysics, 2012, 41: 429-452.
[38] Dušan P., Shina Caroline Lynn K. Molecular modeling of conformational dynamics and its role in enzyme evolution. Current Opinion in Structural Biology, 2018, 52: 50-57.
[39] J.M. Wang, P. Morin, W. Wang, and P.A. Kollman, Use of MM-PBSA in reproducing the binding free energies to HIV-1 RT of TIBO derivatives and predicting the binding mode to HIV-1 RT of efavirenz by docking and MM-PBSA, J. Am. Chem. Soc. 123 (2001), 5221–5230.
[40] W. Wang and P.A. Kollman, Free energy calculations on dimer stability of the HIV protease using molecular dynamics and a continuum solvent model, J. Mol. Biol. 303 (2000), 567–582.
[41] David C. C., Jacobs D. J.: Principal Component Analysis: A Method for Determining the Essential

ISSN 2616-5791 Vol.4, Issue 5: 37-48, DOI: 10.25236/AJMHS.2023.040507

Dynamics of Proteins. Methods Mol Biol 2014, 1084:193-226.
[42] Chen J., Wang L., Wang W., Sun H., Pang L., Bao H.: Conformational transformation of switch domains in GDP/K-Ras induced by G13 mutants: An investigation through Gaussian accelerated molecular dynamics simulations and principal component analysis. Comput Biol Med 2021, 135:104639.
[43] Arnold G. E., Ornstein R. L.: Molecular dynamics study of time-correlated protein domain motions and molecular flexibility: cytochrome P450BM-3. Biophysical Journal 1997, 73:1147-1159.
[44] Fataftah H., Karain W.: Detecting protein atom correlations using correlation of probability of recurrence. Proteins: Structure, Function, and Bioinformatics 2014, 82:2180-2189.
[45] Jakalian A., Bush B. L., Jack D. B., Bayly C. I. Fast, efficient generation of high-quality atomic charges. AM1-BCC model: I. Method. Journal of Computational Chemistry, 2000, 21(2): 132-146.
[46] Jakalian A., Jack D. B., Bayly C. I. Fast, efficient generation of high-quality atomic charges. AM1-BCC model: II. Parameterization and validation. Journal of Computational Chemistry, 2002, 23(16): 1623-1641.
[47] Jorgensen W. L., Chandrasekhar J., Madura J. D., et al. Comparison of simple potential functions for simulating liquid water. Journal of Chemical Physics, 1983, 79(2): 926-935.
[48] Maier J. A., Martinez C., Kasavajhala K., et al. ff14SB: IMcl-1ving the Accuracy of Protein Side Chain and Backbone Parameters from ff99SB. Journal of Chemical Theory and Computation, 2015, 11(8): 3696-3713.
[49] Wang J., Wolf R. M., Caldwell J. W., et al. Development and testing of a general amber force field. Journal of Computational Chemistry, 2004, 25(9): 1157-1174.
[50] Izaguirre J. A., Catarello D. P., Wozniak J. M., et al. Langevin stabilization of molecular dynamics. Journal of Chemical Physics, 2001, 114(5): 2090-2098.
[51] Ryckaert J. P., Ciccotti G., Berendsen H. J. C. Numerical integration of the cartesian equations of motion of a system with constraints: molecular dynamics of n-alkanes. Journal of Computational Physics, 1977, 23(3): 327-341.
[52] Darden T., York D., Pedersen L. Particle mesh Ewald: An N·log(N) method for Ewald sums in large systems. Journal of Chemical Physics, 1993, 98(12): 10089-10092.
[53] Essmann U., Perera L., Berkowitz M. L., et al. A smooth particle mesh Ewald method. Journal of Chemical Physics, 1995, 103(19): 8577-8593.
[54] Weiser J., Shenkin P. S., Still W. C. Approximate atomic surfaces from linear combinations of pairwise overlaps (LCPO). Journal of Computational Chemistry, 1999, 20(2): 217-230.
[55] Götz A. W., Williamson M. J., Xu D., et al. Routine Microsecond Molecular Dynamics Simulations with AMBER on GPUs. 1. Generalized Born. Journal of Chemical Theory and Computation, 2012, 8(5): 1542-1555.
[56] Salomon-Ferrer R., Götz A. W., Poole D., et al. Routine Microsecond Molecular Dynamics Simulations with AMBER on GPUs. 2. Explicit Solvent Particle Mesh Ewald. Journal of Chemical Theory and Computation, 2013, 9(9): 3878-3888.
[57] J. Su, X. Liu, S. Zhang, F. Yan, Q. Zhang, and J. Chen, A computational insight into binding modes of inhibitors XD29, XD35, and XD28 to bromodomain-containing protein 4 based on molecular dynamics simulations, J. Biomol. Struct. Dyn. 36 (2018), 1212–1224.
[58] L. Duan, X. Liu, and J.Z.H. Zhang, Interaction entropy: A new paradigm for highly efficient and reliable computation of protein–ligand binding free energy, J. Am. Chem. Soc. 138 (2016), 5722–5728.
[59] J. Chen, X. Liu, S. Zhang, J. Chen, H. Sun, L. Zhang, and Q. Zhang, Molecular mechanism with regard to the binding selectivity of inhibitors toward FABP5 and FABP7 explored by multiple short molecular dynamics simulations and free energy analyses, Phys. Chem. Chem. Phys. 22 (2020), 2262–2275.
[60] F. Yan, X. Liu, S. Zhang, J. Su, Q. Zhang, and J. Chen, Molecular dynamics exploration of selectivity of dual inhibitors 5M7, 65X, and 65Z toward fatty acid binding proteins 4 and 5, Int. J. Mol. Sci. 19 (2018), 2496.
[61] S. Tian, J. Zeng, X. Liu, J. Chen, J.Z.H. Zhang, and T. Zhu, Understanding the selectivity of inhibitors toward PI4KIIIα and PI4KIIIβ based molecular modeling, Phys. Chem. Chem. Phys. 21 (2019), 22103–22112.
[62] H. Gohlke, C. Kiel, and D.A. Case, Insights into protein–protein binding by binding free energy calculation and free energy decomposition for the Ras–Raf and Ras–RalGDS complexes, J. Mol. Biol. 330 (2003), 891–913.
[63] B. Xu, H. Shen, X. Zhu, and G. Li, Fast and accurate computation schemes for evaluating vibrational entropy of proteins, J. Comput. Chem. 32 (2011), 3188–3193.